J Nanopart Res (2014) 16:2281
DOI 10.1007/s11051-014-2281-x

RESEARCH PAPER

In situ fabrication of Ag nanoparticles/attapulgite nanocomposites: green synthesis and catalytic application

Wenbo Wang · Yuru Kang · Aiqin Wang

Received: 9 September 2013 / Accepted: 15 January 2014 / Published online: 1 February 2014

Abstract A facile solvents-free reaction method was employed to in situ prepare Ag nanoparticles/attapulgite (Ag-NPs/APT) nanocomposites and used for the catalytic reducing decoloration of Congo red (CR) dye. The Ag-NPs with different sizes and loading amounts were in situ formed by the thermal decomposition of silver acetate with no need of any chemical solvent, reductant, stabilizer, or electric current; and the formed Ag-NPs were uniformly immobilized on APT as shown by X-ray diffraction and transmission electron microscopy analyses. The nanocomposites show excellent catalytic activity to catalytic reducing CR dye in the presence of $NaBH_4$, and the CR solution (20 mg/L) can be rapidly decolored within 2 min at the lower dosage of nanocomposite (0.3 g/L). The electron transfer from BH_4^- to the electron acceptor CR, mediated by Ag-NPs, represents the main reduction mechanism. The nanocomposite still shows better catalytic activity after ten cycles, hence it can be used as a recycle material for catalytic applications.

Keywords Ag nanoparticles · Attapulgite · Nanocomposite · Catalytic · Solid-phase reaction

Introduction

In the recent years, the decoration of silver nanoparticles (Ag-NPs) onto a nanocarrier has opened a new avenue to prevent the aggregation of Ag-NPs and obtain the desirable hybrid properties superior to the single one. Thus far, various materials including carbon nanotube (Sahoo et al. 2011; Yan et al. 2011), graphene (Xu and Hu 2012; Das et al. 2011), nanofibers (Mahanta and Valiyaveettil 2012; Sui et al. 2012), silica spheres (Rameshkumar et al. 2013), silica fiber (Patel et al. 2007), nanosheets (Lin et al. 2012), and clays (Shameli et al. 2010; Zhang et al. 2013; Praus et al. 2010; Cabal et al. 2010; Huang and Yang 2008) have been employed as the supporters to fabricate Ag-loaded nanocomposites for antibacterial, catalysis, and biomedical applications. Of these, natural clay minerals are especially concerned owing to their stable crystalline structures, larger surface areas, and plentiful surface groups as well as the abundance, low cost, and eco-friendly advantages (Chiu et al. 2011), and the materials based on silicate clays have been honored as the materials "in greening

Electronic supplementary material The online version of this article (doi:10.1007/s11051-014-2281-x) contains supplementary material, which is available to authorized users.

W. Wang · Y. Kang · A. Wang (✉)
Center of Eco-material and Green Chemistry, Lanzhou Institute of Chemical Physics, Chinese Academy of Sciences, Lanzhou 730030, People's Republic of China
e-mail: aqwang@licp.cas.cn

W. Wang · Y. Kang · A. Wang
R&D Center of Xuyi Attapulgite Applied Technology, Lanzhou Institute of Chemical Physics, Chinese Academy of Sciences, Lanzhou 730000, People's Republic of China

21st century" (Ray and Bousmina 2005). So, many Ag-NPs/clays nanocomposites have been developed (Shameli et al. 2010; Zhang et al. 2013; Praus et al. 2010; Cabal et al. 2010; Huang and Yang 2008), and it was found that the nanoparticles with ideal size distribution and without aggregation can be effectively produced on clay.

Attapulgite (APT, called as palygorskite) is a naturally available one-dimensional nanoscale silicate clay mineral with the 2:1 layer-ribbon structure, special nanorod-like crystal, nanometer channel, and plentiful Si–OH groups (Drits and Sokolova 1971). It has been widely used as the additives of nanocomposite (Huang et al. 2012), adsorbents (He et al. 2011), colloidal agents (Xu et al. 2011), and the supporter of active nanomaterials (Huo and Yang 2012). As a carrier, the greater aspect ratio, surface activity, and charges of APT make it prone to attach metal ions, and then generate hybrid materials loaded with nanoparticles (Lee et al. 2009). Generally, the Ag-NPs/APT nanocomposites were prepared by a chemical reduction and co-precipitation method in liquid phase, and so the usage of solvents, chemical reductants, and stabilizer are required (Liang et al. 2011; Shankar et al. 2011). In addition, the materials produced from a liquid-phase reaction must be separated, dried, and ground to obtain the usable product. Therefore, developing a solvent-free approach of fabricating Ag-NPs/clays hybrid materials becomes the subject of great interests.

Compared with the traditional chemical or electrochemical reduction methods, the pyrolysis of metal salts is a simple and efficient approach to prepare metal-loaded hybrid materials (Burda et al. 2005; Redl et al. 2004). This method has many advantages: (i) the nanomaterials can be in situ formed by a simple one-step thermal decomposition process; (ii) this process does not need chemical solvents, reductants, stabilizer, or electric current. Based on this, the nanoparticles/carbon nanotube nanocomposites have been prepared, and the satisfactory shape and size distribution of nanoparticles were achieved (Yao et al. 2006; Lin et al. 2009). However, the solid-phase reaction approach is rarely used to decorate Ag-NPs onto natural clays to the best of our knowledge.

Herein, we employed a facile approach to decorate Ag-NPs onto APT using AgOAc as the Ag-precursor. The AgOAc was first attached on APT via a mechanical grinding process, and then the AgOAc was thermally decomposed under inert atmosphere to generate Ag-NPs on APT. The developed method of preparing Ag-NPs/APT is based on a simple solid-phase reaction, with no need of any chemical solvent, reductant, and stabilizer. The structure and morphology of the nanocomposites were characterized by X-ray diffraction (XRD) and transmission electron microscopy (TEM) techniques, and their catalytic activities were evaluated by the catalytic reduction reaction of Congo red (CR) dye.

Experimental

Materials

APT, with the chemical composition of CaO 1.29 %, Al_2O_3 9.69 %, Na_2O 0.48 %, MgO 10.94 %, SiO_2 51.75 %, 0.99 % K_2O, and 5.04 % Fe_2O_3, was produced from Mingguang Mine located on Anhui Province, China. Silver acetate (AgOAc, A.R. grade) was purchased from Tianjin Kermel Chemical Reagent Co., Ltd (Tianjin, China). CR was purchased from Alfa Aesar and used without further purification. Sodium borohydride ($NaBH_4$) was purchased from Sinopharm Chemical Reagent Co., Ltd. (Shanghai, China). All the other reagents were of analytical grade and all the solutions were prepared with distilled water.

Preparation of Ag-NPs/APT nanocomposites

The Ag-NPs/APT nanocomposites with the Ag loading amount of 1.0, 2.5, 5, and 10 wt % were prepared by the solid-phase reaction. Typically, the ultrafine AgOAc powder was fully mixed with 1.0 g of APT powder (200 mesh) in an agate mortar, and then the mixture was ground for 30 min to reach a uniform attachment of AgOAc on APT. Subsequently, the ground mixture was calcined in a tube furnace at 300 °C for 2 h under Ar atmosphere. After natural cooling to room temperature, the black powder product was collected for further use.

Evaluation of catalytic activities

The catalytic activities of the nanocomposites were evaluated by the catalytic reduction reaction of CR in the presence of $NaBH_4$. Typically, 0.03 g of the Ag-NPs/APT nanocomposites was added into 100 mL of

the CR solution (20 mg/L) with 15 mmol/L of $NaBH_4$. After set time intervals (10, 20, 30, 60, 120, 180, 300, and 480 s), the nanocomposites were instantly separated from the solution by a filter (0.45 μm), and the UV–Vis spectra of the filtrate were scanned at 25 °C in a range of 300–700 nm. The maximum absorbance wavelength is 504 nm, and the absorbance of the solution was determined at this wavelength using a quartz cell (1 cm path length). The change of absorbance before and after catalytic reduction was defined as the criterion to evaluate the decoloration efficiency. The nanocomposite was collected, washed with distilled water for three times, dried under vacuum, and then used for another catalytic cycle. The same procedure was repeated 10 times to evaluate the reusability of the nanocomposites.

Calculation of reduction rate constants

The catalytic reduction rate of CR in the presence of $NaBH_4$ was calculated using the following Eq. (1).

$$-\ln(C/C_0) = K_{obs}t, \quad (1)$$

where C (mg/L) is the concentration of CR dye at time t, C_0 (mg/L) is the initial concentration of CR dye, and K_{obs} is the first-order rate constant (Bokare et al. 2008).

Characterizations

XRD patterns were collected on an X'pert PRO X-ray power diffractometer (PAN analytical Co., the Netherlands) using Cu-Kα radiation of 0.1541 nm (40 kV, 30 mA). The TEM images were taken using a JEM-2010 high-resolution TEM (JEOL, Tokyo, Japan) at an acceleration voltage of 200 kV, and the sample was ultrasonically dispersed in anhydrous ethanol and dropped onto a micro grid before observation. UV–Vis spectra were determined using a SPECORD 200 UV–visible spectrophotometer (Analytik Jera AG).

Results and discussion

Formation of Ag-NPs/APT nanocomposites

APT has been taken as the ideal supporter of metal nanoparticles to derive various nanocomposites by virtue of its higher aspect ratio, specific surface area, and surface activity as well as the abundance, low cost, and eco-friendly advantages. However, the conventional approach of fabricating Ag-NPs/APT nanocomposite is mainly based on a liquid-phase reaction, and the usage of chemical solvents, reductants, and stabilizer is unavoidable. Hence, we developed a facile solid-phase reaction method to in situ produce Ag-NPs on APT substrate and form Ag-NPs/APT nanocomposites (Fig. 1). The ultrafine AgOAc was mixed with APT and then manually ground for 30 min to achieve a uniform attachment of AgOAc on APT. The ground mixture was heated to 300 °C at the heating rate of 10 °C/min, and then kept at 300 °C for 2 h under an Ar atmosphere. The AgOAc can be thoroughly decomposed at 300 °C to form Ag-NPs. It has also been confirmed that the thermal decomposition product of AgOAc is Ag^0 (Logvinenko et al. 2007; Afzal et al. 1991), and so AgOAc has been used as the Ag-precursor to produce Ag^0 nanomaterials (Abdullayev et al. 2011; Jeevanandam et al. 2010; Uznanski and Bryszewska 2010). We also analyzed the thermal decomposition product of the ground AgOAc (without APT) at 300 °C by XRD (Fig. S1, see Supplementary Information) and TEM (Fig. S2, see Supplementary Information), and the expected results were observed: the thermal decomposition of AgOAc can generate Ag^0 (Fig. S1, see Supplementary Information) (JCPDF No. 87-0720) through a self-reduction process with no assist of any reductants (Logvinenko et al. 2007; Afzal et al. 1991; Abdullayev et al. 2011; Jeevanandam et al. 2010; Uznanski and Bryszewska 2010). TEM result indicates that the thermal decomposition of AgOAc fails to form uniform nanoparticles with better shape and size

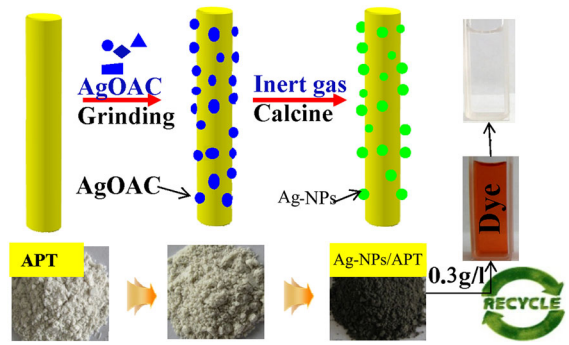

Fig. 1 Schematic representation for the formation of Ag-NPs/APT nanocomposites

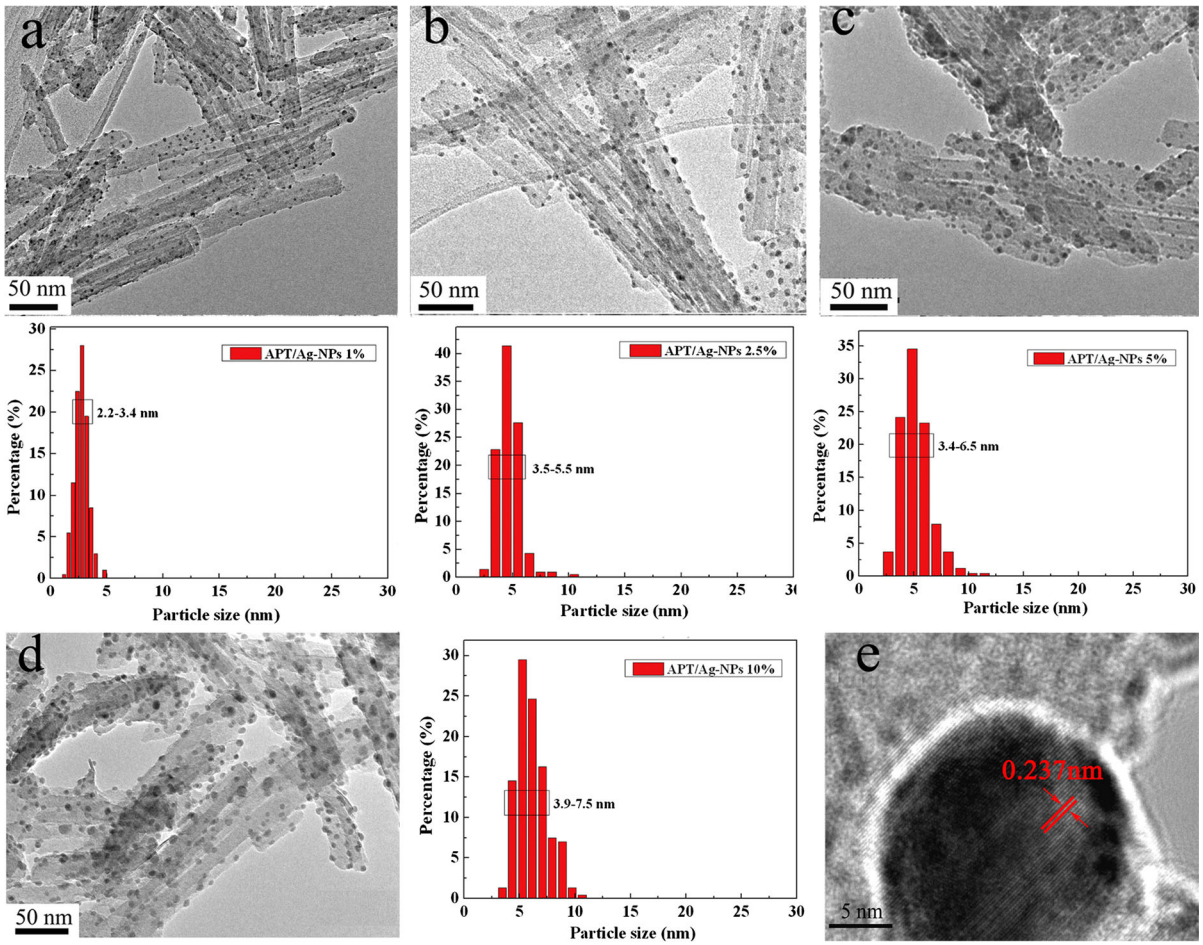

Fig. 2 TEM images of Ag-NPs/APT with 1 wt% (**a**), 2.5 wt% (**b**), 5 wt% (**c**), and 10 wt% (**d**) of Ag loading amounts, and the HRTEM of the Ag-NPs (**e**). The *histogram* is the corresponding size distribution from the statistics of 200 particles on TEM images

distribution, and only bulk or macroparticles were observed (Logvinenko et al. 2007) (Fig. S2, see Supplementary Information).

TEM analysis

Figure 2 shows the TEM images of Ag-NPs/APT with different loading amounts of Ag as well as the size distribution of Ag-NPs on APT. As can be seen, the spherical or quasi spherical Ag-NPs were observed on the APT nanorods (with the length of about 500 nm–1 μm), which provide a visible evidence for the formation of Ag-NPs on APT supporter after thermal treatment. The in situ formed Ag-NPs were anchored and uniformly distributed on APT without obvious aggregation. Compared with the TEM image of the thermal decomposition product of AgOAc (without APT) (Fig. S2), the Ag-NPs on APT have relatively better spherical shape and narrow particle size distribution (Fig. 2). This indicates that APT nanorods are essential to obtain an ideal shape and size of Ag-NPs and can be used as a suitable supporter to immobilize Ag-NPs and prevent their aggregation. The size distribution of Ag-NPs is in the range of 2.2–3.4 nm when the Ag loading is 1 % (Fig. 2a). With increasing the loading amount of Ag, the size of main particles was gradually increased. The size distribution is in the range of 3.5–5.5 nm for 2.5 % Ag, 3.4–6.5 nm for 5 % Ag, and 3.9–7.5 nm for 10 % Ag (Fig. 2b–d). Comparatively, the size distribution of particles is

relatively narrow when the loading amount of Ag is lower than 2.5 %; whereas it becomes wide with increasing the loading of Ag above 2.5 % (Fig. 2c, d). The lattice fringe spacing of the obtained Ag nanocrystal is 0.237 nm (Fig. 2e), which is consistent with the XRD results and confirmed the formation of Ag-NPs.

The formation of Ag-NPs involves the nucleation step and growth step. APT has numerous surface Si–OH, Al–OH, Si–O^-, and Al–O^- groups with negative charges (Drits and Sokolova 1971). These groups may anchor with the dissociated Ag^+ during the thermal decomposition of AgOAc. When the temperature was increased to 180–300 °C (Afzal et al. 1991), the tiny Ag^0 nanocrystals was generated and acted as a nuclear to induce the growth of Ag^0 crystals (Abdullayev et al. 2011; Jeevanandam et al. 2010; Uznanski and Bryszewska 2010), and thus the spherical Ag-NPs can be formed on APT.

XRD analysis

The XRD analysis provided a direct evidence for the formation of Ag-NPs/APT nanocomposites. As shown in Fig. 3, APT shows the characteristic diffraction peaks at $2\theta = 8.42°$ ($d = 1.0505$ nm; 1 1 0 plane), $2\theta = 13.75°$ ($d = 0.6435$ nm, 2 0 0 plane), $2\theta = 16.42°$ ($d = 0.5394$ nm, 1 3 0 plane), $2\theta = 19.89°$ ($d = 0.4460$ nm, 0 4 0 plane), $2\theta = 21.48°$ ($d = 0.4134$ nm, 3 0 0 plane), and $2\theta = 24.25°$ ($d = 0.3667$ nm, 2 4 0 plane). After heat treatment, the diffraction peaks of Ag^0 appear at $2\theta = 38.22°$ ($d = 0.2370$ nm, 1 1 1 plane) and 44.29° ($d = 0.2044$ nm, 2 0 0 plane) (Liang et al. 2011) (JCPDF No. 87-0720), indicating that the thermal decomposition of AgOAc generated face-centered cubic Ag-NPs (space groups, Fm3m) on APT. As expected, no diffraction peak of AgO (JCPDF No. 84-1108) and AgOAc can be observed, indicating that AgOAc was completely decomposed and no AgO by-product was formed (Jeevanandam et al. 2010; Uznanski and Bryszewska 2010). With increasing the loading amount of Ag, the intensity of diffraction peaks was gradually increased, which is consistent with the XRF spectra of the nanocomposite (Fig. S3, see Supplementary Information). Whereas, the position of 1 1 0 diffraction peaks of APT has no obvious change, which indicates that the crystal structure of APT was not destroyed during the heat-treatment process.

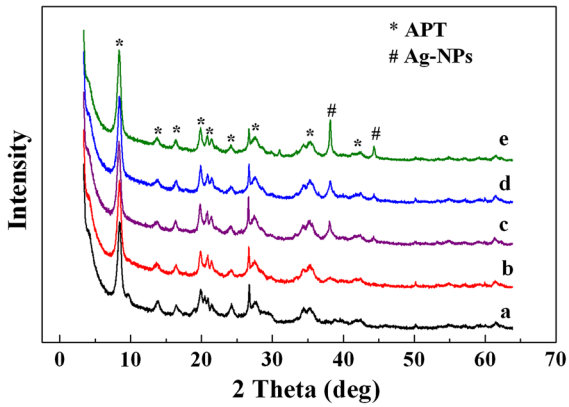

Fig. 3 XRD patterns of APT (*a*) and Ag-NPs/APT with 1 wt% (*b*), 2.5 wt% (*c*), 5 wt% (*d*), and 10 wt% (*e*) of Ag loading amounts

Catalytic properties

The immobilization of Ag-NPs onto APT endows the nanocomposites with satisfactory catalytic activity. The catalytic reduction reaction of the anionic dye CR in the presence of $NaBH_4$ was used to evaluate the catalytic properties of Ag-NPs/APT. CR was chosen as the model dye because its maximum absorbance wavelength (504 nm) is not overlapped with the plasmon band of silver (~410 nm) and its reduction product is colorless. As shown in Fig. 4a, the addition of $NaBH_4$ to CR solutions does not change the absorbance, which indicates that single BH_4^- ion cannot reduce the CR dye in the absence of catalyst. Also, the addition of the Ag-NPs/APT alone also fails to decolor the CR solution in the absence of BH_4^-, and only weaker absorption of APT for CR dye was observed. However, the simultaneous addition of Ag-NPs/APT nanocomposite and BH_4^- ions rapidly decolored the CR solution (inset in Fig. 4b), and the absorbance was rapidly decreased to the value close to zero. In order to calculate the rate constant K_{obs}, the experimental data were fitted with Eq. (1). It can be seen that the plots of $-\ln(C_t/C_0)$ versus t give better straight lines (Fig. S4, see Supplementary Information), and the slope is equal to the K_{obs} value. The K_{obs} values are 0.1730, 0.1921, 0.2214, and 0.2246 s^{-1} for Ag-NPs/APT with 1, 2.5, 5, and 10 % Ag loadings, respectively.

When the loading amount of Ag is lower than 5 %, the reduction rate increased with increasing the loading amount of Ag (the dosage of Ag-NPs/APT is 0.3 g/L). When the loading amount of Ag is equal to or greater than 5 %, the further increase of the loading amount of

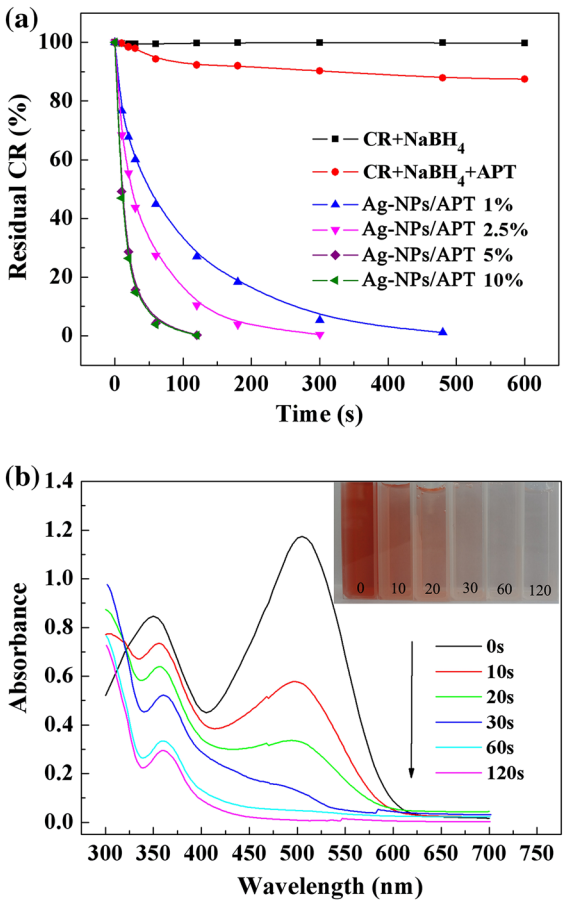

Fig. 4 **a** Catalytic reduction kinetic curves of the Ag-NPs/APT for CR solution (initial CR concentration, 20 mg/L; initial $NaBH_4$ concentration, 15 mmol/L; and initial dosage, 0.3 g/L); and **b** the corresponding UV–Vis spectra for the catalytic reduction of CR using Ag-NPs/APT (5 %) as the catalyst. The *inset* in **b** is the digital photo of the decoloration of CR

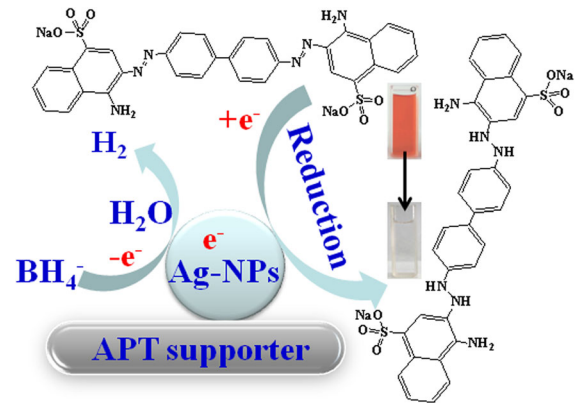

Fig. 5 Proposed mechanisms for the catalytic reduction of CR by $NaBH_4$ using Ag-NPs/APT as the catalyst

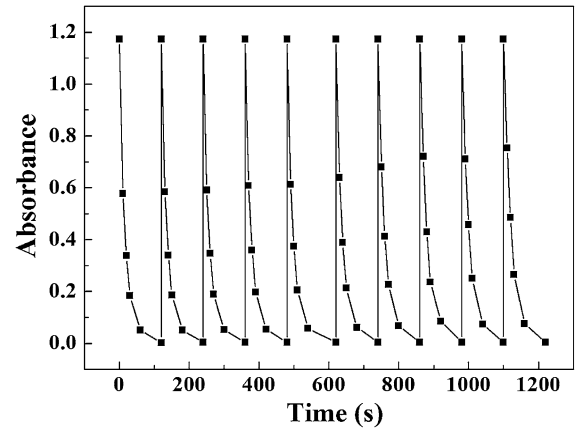

Fig. 6 Catalytic kinetics of CR for ten successive cycles with the same batch of Ag-NPs/APT nanocomposite (initial CR concentration, 20 mg/L; initial $NaBH_4$ concentration, 15 mmol/L; and initial dosage, 0.3 g/L)

Ag has no obvious contribution to the reduction rate. This indicates that Ag-NPs play a key role to the catalytic reduction of CR, and the Ag loading of 1–5 % is suitable for the practical application.

In the process of catalytic reaction, the Ag-NPs trigger the reduction of CR solution by relaying electrons from the BH_4^-donor to Ag-NPs, and then conveying the electrons to the acceptor CR molecules (Li et al. 2013). As a result, the azo double –N=N– bonds were reduced as the –N–N– bonds, and the color of CR faded (Fig. 5) (Vidhu and Philip 2014).

It can also been seen that the plasmon bands of silver (~410 nm) are not observed in the UV–Vis absorbance spectra of CR solution after catalytically reducing by $NaBH_4$ (Fig. 4b), which indicates that no detachment phenomenon occurred and Ag-NPs can stably anchor on APT. Moreover, the nanocomposite shows excellent reusability when it was reused for 10 cycles (Fig. 6). It can be observed that the initial reduction rate was decreased with increasing the reuse times, especially the cycle times is above 6 times, whereas the final catalytic efficiency has no obvious reduction. This indicates that the nanocomposite can be used as potential and promising reusable catalysis materials.

Conclusions

The fabrication of various usable new materials by adopting new methods plays vital roles in the modern

academic and industrial fields. Especially in the recent years, the "greening" of material itself and its preparation methods attracted global attention and became the research focus. Ag-NPs are promising materials with excellent properties and extensive applications, and the Ag-NPs/clays also show satisfactory performance and eco-friendly characteristics. However, such materials have usually been prepared by complex liquid-phase reaction, which needs to use various solvents, chemical reductants, and stabilizers with environmental risk. Thus, a facile and efficient solid-phase reaction approach was developed to in situ fabricate Ag-NPs/APT nanocomposite. In this process, the Ag-NPs with a spherical shape were formed and anchored on APT (as proven by XRD and TEM analysis) through a simple grinding–heating process. The nanocomposite shows excellent catalytic reducing properties for dye, which can rapidly decolor the CR solution (20 mg/L) within 2 min (Ag-NPs/APT 5 %) only using a low dosage of catalyst (0.3 g/L), and so the materials are suitable catalyst for the treatment of CR dye wastewater. As a whole, it is expected that this study provides a new approach to design metallic nanoparticles/clay nanocomposites with satisfactory performance and eco-friendly advantages for efficient and promising catalysis applications.

Acknowledgments The authors would like to thank the Science and Technology Support Project of Jiangsu Provincial Sci. & Tech. Department (No. BE2012113) and "863" Project of the Ministry of Science and Technology, P. R. China (No. 2013AA031403) for the financial support of this research.

References

Abdullayev E, Sakakibara K, Okamoto K, Wei WB, Ariga K, Lvov Y (2011) Natural tubule clay template synthesis of silver nanorods for antibacterial composite coating. ACS Appl Mater Interface 3:4040–4046

Afzal M, Butt PK, Ahrnad H (1991) Kinetics of thermal decomposition of metal acetates. J Therm Anal 37: 1015–1023

Bokare AD, Chikate RC, Rode CV, Paknikar KM (2008) Iron–nickel bimetallic nanoparticles for reductive degradation of azo dye Orange G in aqueous solution. Appl Catal B: Environ 79:270–278

Burda C, Chen X, Narayanan R, El-Sayed MA (2005) Chemistry and properties of nanocrystals of different shapes. Chem Rev 105:1025–1102

Cabal B, Torrecillas R, Malpartida F, Moya JS (2010) Heterogeneous precipitation of silver nanoparticles on kaolinite plates. Nanotechnology 21:475705

Chiu CW, Hong PD, Lin JJ (2011) Clay-mediated synthesis of silver nanoparticles exhibiting low-temperature melting. Langmuir 27:11690–11696

Das MR, Sarma RK, Saikia R, Kale VS, Shelke MV, Sengupta P (2011) Synthesis of silver nanoparticles in an aqueous suspension of graphene oxide sheets and its antimicrobial activity. Colloids Surf B: Biointerface 83:16–22

Drits VA, Sokolova GV (1971) Structure of palygorskite. Sov Phys Crystallogr 16:183–185

He MY, Zhu Y, Yang Y, Han BP, Zhang YM (2011) Adsorption of cobalt(II) ions from aqueous solutions by palygorskite. Appl Clay Sci 54:292–296

Huang HT, Yang Y (2008) Preparation of silver nanoparticles in inorganic clay suspensions. Compos Sci Technol 68: 2948–2953

Huang DJ, Wang WB, Xu JX, Wang AQ (2012) Mechanical and water resistance properties of 1 chitosan/poly (vinyl alcohol) films reinforced with attapulgite dispersed by high-pressure homogenization. Chem Eng J 210:166–172

Huo CL, Yang HM (2012) Attachment of nickel oxide nanoparticles on the surface of palygorskite nanofibers. J Colloid Interface Sci 384:55–60

Jeevanandam P, Srikanth CK, Dixit S (2010) Synthesis of monodisperse silver nanoparticles and their self-assembly through simple thermal decomposition approach. Mater Chem Phys 122:402–407

Lee JA, Krogman KC, Ma M, Hill RM, Hammond PT, Rutledge GC (2009) Highly reactive multilayer-assembled TiO_2 coating on electrospun polymer nanofibers. Adv Mater 21:1252–1256

Li W, Li J, Qiang WB, Xu JJ, Xu DK (2013) Enzyme-free colorimetric bioassay based on gold nanoparticle-catalyzed dye decolorization. Analyst 138:760–766

Liang F, Liu BZ, Deng YH, Yang SG, Sun C (2011) Preparation and characterization of attapulgite-silver nanocomposites, and their application to the electrochemical determination of nitrobenzene. Microchim Acta 174:407–412

Lin Y, Watson KA, Fallbach MJ, Ghose S, Smith JG, Delozier JDM, Cao W, Crooks RE, Connell JW (2009) Rapid, solventless, bulk preparation of metal nanoparticle-decorated carbon nanotubes. ACS Nano 3: 871–884

Lin Y, Bunker CE, Fernando KAS, Connell JW (2012) Aqueously dispersed silver nanoparticle-decorated boron nitride nanosheets for reusable, thermal oxidation-resistant surface enhanced Raman spectroscopy (SERS) devices. ACS Appl Mater Interface 4:1110–1117

Logvinenko V, Polunina O, Mikhailov Y, Mikhailov K, Bokhonov B (2007) Study of thermal decomposition of silver acetate. J Therm Anal Calorim 90:813–816

Mahanta N, Valiyaveettil S (2012) In situ preparation of silver nanoparticles on biocompatible methacrylated poly (vinyl alcohol) and cellulose based polymeric nanofibers. RSC Adv 2:11389–11396

Patel AC, Li SX, Wang C, Zhang WJ, Wei Y (2007) Electrospinning of porous silica nanofibers containing silver nanoparticles for catalytic applications. Chem Mater 19:1231–1238

Praus P, Turicová M, Machovič V, Študentová S, Klementová M (2010) Characterization of silver nanoparticles deposited on montmorillonite. Appl Clay Sci 49:341–345

Rameshkumar P, Manivannan S, Ramaraj R (2013) Silver nanoparticles deposited on amine-functionalized silica spheres and their amalgamation-based spectral and colorimetric detection of Hg(II) ions. J Nanopart Res 15:1639

Ray SS, Bousmina M (2005) Biodegradable polymers and their layered silicate nanocomposites: in greening the 21st century materials world. Prog Mater Sci 50:962–1079

Redl FX, Black CT, Papaefthymiou GC, Sandstrom RL, Yin M, Zeng H, Murray CB, O'Brien SP (2004) Magnetic, Electronic, and structural characterization of nonstoichiometric iron oxides at the nanoscale. J Am Chem Soc 126: 14583–14599

Sahoo S, Husale S, Karna S, Nayak SK, Ajayan PM (2011) Controlled assembly of Ag nanoparticles and carbon nanotube hybrid structures for biosensing. J Am Chem Soc 133:4005–4009

Shameli K, Ahmad MB, Yunus WZW, Ibrahim NA, Darroudi M (2010) Synthesis and characterization of silver/talc nanocomposites using the wet chemical reduction method. Int J Nanomed 5:743–751

Shankar R, Groven L, Amert A, Whites KW, Kellar JJ (2011) Non-aqueous synthesis of silver nanoparticles using tin acetate as a reducing agent for the conductive ink formulation in printed electronics. J Mater Chem 21:10871–10877

Sui CH, Li C, Guo XH, Cheng TX, Gao YK, Zhou GD, Gong J, Du JS (2012) Facile synthesis of silver nanoparticles-modified PVA/$H_4SiW_{12}O_{40}$ nanofibers-based electrospinning to enhance photocatalytic activity. Appl Surf Sci 258:7105–7111

Uznanski P, Bryszewska E (2010) Synthesis of silver nanoparticles from carboxylate precursors under hydrogen pressure. J Mater Sci 45:1547–1552

Vidhu VK, Philip D (2014) Catalytic degradation of organic dyes using biosynthesized silver nanoparticles. Micron 56:54–62

Xu ZX, Hu GX (2012) Simple and green synthesis of monodisperse silver nanoparticles and surface-enhanced Raman scattering activity. RSC Adv 2:11404–11409

Xu JX, Zhang JP, Wang Q, Wang AQ (2011) Disaggregation of palygorskite crystal bundles via high-pressure homogenization. Appl Clay Sci 54:118–123

Yan Y, Sun HP, Yao PP, Kang SZ, Mu J (2011) Appl Surf Sci 257:3620–3626

Yao YL, Ding Y, Ye LS, Xia XH (2006) Two-step pyrolysis process to synthesize highly dispersed Pt–Ru/carbon nanotube catalysts for methanol electrooxidation. Carbon 44:61–66

Zhang YT, Chen YF, Zhang HQ, Zhang B, Liu JD (2013) Potent antibacterial activity of a novel silver nanoparticle–halloysite nanotube nanocomposite powder. J Inorg Biochem 118:59–64